ChemComm

Accepted Manuscript

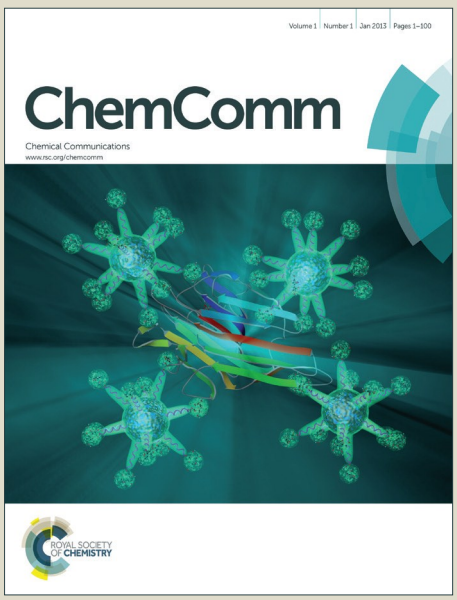

ROYAL SOCIETY OF CHEMISTRY

www.rsc.org/chemcomm

Journal Name

COMMUNICATION

$FeCo_2O_4$ submicron-tube arrays grown on Ni foam as high rate-capability and cycling-stability electrodes allowing superior energy and power densities with symmetric supercapacitors†

Received 00th January 20xx,
Accepted 00th January 20xx

DOI: 10.1039/x0xx00000x

www.rsc.org/chemcomm

Baogang Zhu,‡ Shaochun Tang,*‡ Sascha Vongehr, Hao Xie, Jian Zhu and Xiangkang Meng*

Template-free chemical growth on Ni foam and thermal treatment results in homogeneous $FeCo_2O_4$ submicron-tube arrays which serve as binder-free electrodes with high capacitance, rate-capability and cycling-stability owing to $FeCo_2O_4$ conductivity, high porosity, and strong bonding between tubes and Ni foam, all allowing even symmetric devices to have superior energy density.

With rapidly increasing demand for electric energy storage, supercapacitors (SCs) have attracted extensive research interest due to their fast recharge capability, high power density and long cycle life.[1] Transition metal (Ni, Co, Mn, etc.) oxides are widely explored as active materials for SCs based on reversible redox reactions because of their low cost, low toxicity, and high theoretical capacitances (> 1000 F/g).[2] However, their conductivity is typically too low to support fast electron transport, which decreases the rate capability.[3] Mixed transition metal oxides such as MCo_2O_4 (M = Ni[4], Cu[5] and Zn[6]) perform well owing to their multiple oxidation states and much higher electrical conductivity. $NiCo_2O_4$ exhibits a by 2 orders of magnitude higher electric conductivity than nickel or cobalt oxides.[7] Since Co oxides[8] and Fe oxides[9] both provide excellent electrochemical performance, Fe-Co oxide ($FeCo_2O_4$) is expected to be an excellent electrode material that offers richer redox reactions than corresponding single components, in much the same way as $NiCo_2O_4$ compared with their single component oxides.[4] So far, research on $FeCo_2O_4$ is limited,[10] but the results on its energy storage properties suggest that its potential in SCs should be further explored.

Electrodes with porous microstructures enhance not only power density but also rate capability, because the porosity increases the electrode/electrolyte contact interface and electrolyte penetration.[11-13] Therefore, developing novel porous architectures is an effective route to achieve high electrochemical performance. Much current research focuses on growing pseudocapacitive materials on three-dimensional conducting backbones such as Ni foam,[14,15] which increases not only electrical conductivity but also mechanical stability. Various synthetic methods such as sacrificial template-accelerated hydrolysis,[16] in-situ sacrificial template,[17] and anion-exchange[18] have been developed to grow tubular nanostructures which are promising because electrochemical reactions may also occur on inner surfaces. These are all focused on nanosized tubes, and the methods are complicated. Submicron/micron-sized porous materials were demonstrated to be excellent electrode materials for SCs due to their sizes for desirable mechanical properties and high cycling stability.[19]

In this communication, novel $FeCo_2O_4$ submicron-tube arrays were grown on Ni foam via a template-free chemical deposition followed by thermal treatment. The tubes are separated from each other and distribute homogeneously on the foam, forming a highly porous structure. Such arrays possess the following advantages: (1) they can be used directly as electrodes, which avoids polymer binder additives; (2) the high porosity leads to excellent specific areal capacitances; (3) the high conductivity of $FeCo_2O_4$ and a good connection between the tubes and the Ni endow the arrays with good electric conductivity and thus good rate capability; (4) and the direct growth results in excellent long-term cycling stability. All-solid-state symmetric supercapacitors were assembled from the novel electrodes and resulted in excellent power and current densities superior to other symmetric devices with similar electrodes. The results instead fit together among asymmetric supercapacitors based on similar mixed oxides.

The preparation procedures are described in detail in the ESI.† SEM and TEM images of the products before thermal treatment (ESI,† Fig. S1a-b) show that hollow tubes are already obtained with 310 ± 20 nm thick walls. TEM (ESI,† Fig. S1c) and HRTEM images (ESI,† Fig. S1d) indicate the single crystalline nature of an individual tube. During the chemical deposition,

*National Laboratory of Solid State Microstructures, College of Engineering Applied Sciences, and Institute of Materials Engineering, Nanjing University, Nanjing 210093, Jiangsu, P. R. China. E-mail: tangsc@nju.edu.cn, mengxk@nju.edu.cn.

† Electronic Supplementary Information (ESI) available: [Experimental details; SEM, TEM, and HRTEM images of the tubes before thermal treatment; XPS spectra of the $FeCo_2O_4$ on Ni foam; SEM images of the $FeCo_2O_4$ grown on Ni foam obtained with different $C_{Fe^{3+}}$.]. See DOI: 10.1039/x0xx00000x ‡

‡ These authors contributed equally to this work.

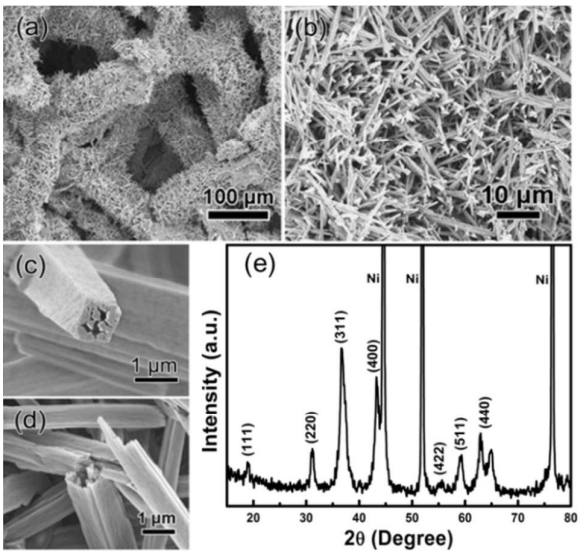

Fig. 1 (a) low- and (b) high-magnification SEM images of typical $FeCo_2O_4$ tubes on Ni foam, (c) SEM image showing one tip of a tube, (d) a broken tube, and (e) XRD pattern of the sample.

fast nucleation and initial growth result in polyhedral sub-micron hollow particles on Ni, and subsequent anisotropic growth along preferred directions leads to single-crystalline submicron tubes. A transformation to resulting $FeCo_2O_4$ during thermal treatment is performed according to the equation:

$$FeCo_2(C_2O_4)_3 + 2O_2 = FeCo_2O_4 + 6CO_2 \uparrow$$

Fig. 1a shows low-magnification SEM image of the typical $FeCo_2O_4$ product. The Ni foam's ligaments are all homogeneously covered but its 3D porous structure is still remained. The tubes are distributed on the ligaments of the Ni foam and separated from each other, forming a highly porous structure (Fig. 1b). Fig. 1c shows that an individual tube's tip is hollow having a polygonal shape with an average polygon edge length of about 700-800 nm. The outer surface is smooth. A cross section of a broken tube (Fig. 1d) demonstrates that the middle section is also hollow and that its cross section is polygonal. The XPS analysis (ESI,† Fig. S2) reveals that Co^{2+} and Co^{3+} exist together and Fe is only in the state of Fe^{2+} in the product. XRD pattern (Fig. 1e) shows that except for three strong peaks due to the Ni substrate, other diffraction peaks can be indexed as $FeCo_2O_4$ spinel phase (Fd3m space group).[10] According to the Scherrer equation $D=0.89\ \lambda/[\beta\cos(\theta)]$, where λ is the x-ray wavelength and β is the full width at half maximum, the average grain size was calculated to be 10.9 nm.

A TEM image (Fig. 2a) shows that the wall thickness has halved during the thermal treatment. This is because during the annealing process in air, an oxidation reaction happens firstly at the surface resulting in a $FeCo_2O_4$ layer, and the inner atoms move to the surface to react with oxygen. The tubes are now polycrystalline (SAED pattern inset) and composed of crystallites of 5-12 nm in diameter (Fig. 2b), which is consistent with the XRD results. HRTEM analysis (Fig. 2c) shows lattice distances of 0.47 and 0.24 nm in various crystal grains (in circled areas), which correspond to the (111) and (311) planes of the $FeCo_2O_4$ cubic phase, respectively. The crystallographic orientations of those grains lie in random directions.

SEM images of the products obtained with different reactants' concentrations (defined as C_{Fe}^{3+}, the concentrations of Co^{2+} and oxalic acid changed correspondingly) are shown in ESI,† Fig. S3. At a low C_{Fe}^{3+} of 1.3 mM, many intersecting thin flakes with ~200 nm diameters cover the Ni foam's ligaments (ESI, † Fig. S3a). Increasing the C_{Fe}^{3+} to 5 mM, many aggregations with irregular shapes form (ESI,† Fig. S3b). Only at around 10 mM (Fig. 1) and 12.5 mM (ESI,† Fig. S3c) are the tubular nanostructures obtained. At and beyond 17.5 mM, the porosity on the micron scale is absent (ESI, † Fig. S3d). According to the TAG results (ESI,† Fig. S4), the loadings of $FeCo_2O_4$ on Ni foams are 0.4, 1.5, 2.6 and 5.9 mg/cm^2 when the C_{Fe}^{3+} values are 5, 10, 12.5, and 17.5 mM, respectively.

The $FeCo_2O_4$-tube arrays covered Ni foams can be directly used as electrodes. Fig. 3a shows the CV curves of the electrodes obtained with different C_{Fe}^{3+} at a scan rate of 40 mV/s. The curves' shapes and redox peaks indicate a pseudocapacitive nature of the charging reactions. The redox current peaks are attributed to the reversible reaction between Co^{2+} and Co^{3+}, Fe^{2+} and Fe^{3+}. The area integrated under the curves changes with the concentration, the largest specific capacitance being at 10 mM. The potential difference between the oxidation peak and the reduction peak is a measure of the irreversibility in the redox reaction. Smaller values correspond to better reversibility.[20] The potential difference is lowest, namely only about 105 mV, at C_{Fe}^{3+} = 10 mM. The CD curves at a current density of 2 mA/cm^2 (Fig. 3b) show that the best galvanostatic charge-discharge performance is also obtained at 10 mM (700 seconds), indicating maximum specific capacitance. The corresponding specific areal capacitances (C_{area}) of the electrodes at different current densities are shown in Fig. 3c. They are again optimal at C_{Fe}^{3+} = 10 mM. The optimum being at 10 mM for all these electrochemical measurements coincides with the homogeneous and highly porous structure characteristics (see the SEM images in ESI,† Fig. S3).

Nyquist plots of three electrodes obtained with low, optimal, and high C_{Fe}^{3+} are shown in Fig. 3d. The equivalent circuit (inset) has a bulk solution resistance R_s, charge-transfer resistance R_{ct} and the Warburg impedance (W). A larger electroactive surface area indicates a lower charge-transfer resistance. R_s is related to the conductivity of the electrolyte and internal resistance of the electrode. The electrode obtained with C_{Fe}^{3+} =10 mM has the lowest R_{ct} = 0.31 Ω and R_s = 1.44 Ω. These values are close to those for the widely

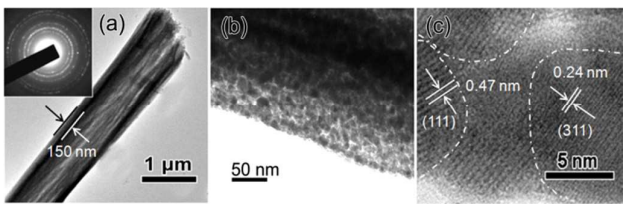

Fig. 2 (a) Low- and (b) high-magnification TEM images (inset is SAED pattern) of a single $FeCo_2O_4$ tube and (c) HRTEM analysis.

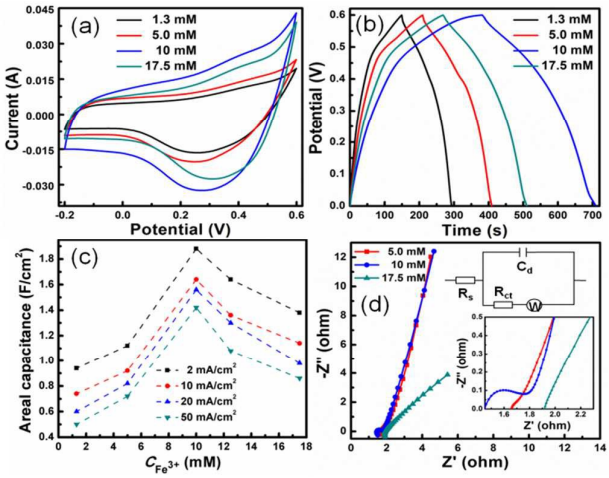

Fig. 3 Comparison of the electrodes gotten with different C_{Fe}^{3+}: (a) CVs at a scan rate of 40 mV/s, (b) CD curves at a current density of 2 mA/cm^2, (c) areal capacitances C_a at different current densities vs. concentration, and (d) EIS curves of three electrodes obtained with low, optimal, and high C_{Fe}^{3+}.

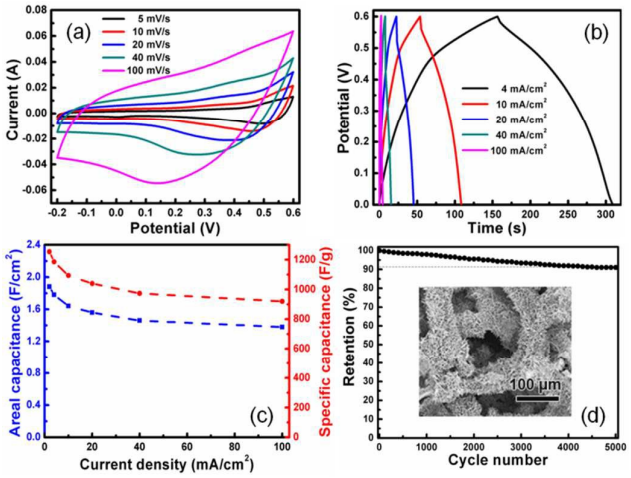

Fig. 4 (a) CV curves of the optimal electrode measured at different scan rates, (b) Galvanostatic CD curves at different current densities, (c) C_a and C_g vs. current density, and (d) cycling performance over 5000 cycles at 10 mA/cm^2.

investigated highly conductive $NiCo_2O_4$,[21] indicating that $FeCo_2O_4$ is also much enhanced in electric conductivity over the corresponding single metal oxides, much like $NiCo_2O_4$. The lowest values of R_{ct} and R_s at the optimized point are consistent with that of specific capacitances. These low values are mainly due to the highly porous structure providing large electroactive surface area, which facilitates ion insertion/extraction during electrochemical reactions. The direct connection between tubes and Ni foam decreases the contact resistance.

Fig. 4a shows CV curves of the optimal electrode at various scan rates. The area inside the curves increases with the scan rate. In CD curves (Fig. 4b), triangular symmetry and near linear slopes reveal excellent electrochemical performance of the optimal electrode. After the maximum, a small but steep potential drop is attributed to the internal resistance of the electrode and ionic resistance of electrolyte.[22] A small drop indicates a low resistance consistent with the EIS results. Fig. 4c illustrates the change of the areal capacitance C_{area} with current density, which is calculated from the discharge curves. The values are 1.88, 1.78, 1.64, 1.56, 1.46 and 1.38 F/cm^2 at 2, 4, 10, 20, 40 and 100 mA /cm^2. Note that they are calculated from selected, linear voltage drop ranges ΔV and corresponding Δt (details in the ESI†). The specific gravimetric capacitances (C_g) are 1254, 1186, 1094, 1040, 974, 920 F/g, respectively. The optimized specific capacitances of the $FeCo_2O_4$-tube electrode are not only higher than reported values for the corresponding single metal iron or cobalt oxides,[8] but also even higher than other mixed metals oxide nanostructures such as $MnCo_2O_4$ nanoparticles,[23] $CuCo_2O_4$ particles,[5] $ZnCo_2O_4$ nanotubes,[6] $NiCo_2O_4$ with different morphologies[7,24,25,26] (ESI,† Table S1). The high C_g is mainly attributed to that the electrolyte can diffuse into the whole porous skeleton of electrode, leading to that all the active material participates in electrochemical reactions. The areal capacitance is still at 1.38 F/cm^2 even at a high current density of 100 mA/cm^2, a 74% capacity retention is much higher than 52% (from 1 to 20 A/g) for $NiCo_2O_4$ nanosheets,[24] and 26% (from 1 to 50 A/g) for $CuCo_2O_4$ particles[5]. The high rate capability is mainly attributed to the homogeneous distribution of tubes and high porosity of the arrays. The cycling life was evaluated by galvanostatic CD measurements. 91% of the initial areal capacitance remained after 5000 cycles at a current density of 10 mA/cm^2 (Fig. 4d), which indicates a superior cycling stability over the above-mentioned MCo_2O_4 (M = Ni[26], Zn[6] and Mn[23]) electrodes. The arrays' porous structure is unchanged after 5000 cycles (see the inset), confirming a high mechanical stability. The high cycling stability is mainly attributed to the strong bonding between tubes and Ni foam, which is demonstrated by that the same morphology and CV shapes of typical $FeCo_2O_4$ tube arrays on Ni foam are unchanged after ultrasound (see ESI,† Fig. S5).

An all-solid-state symmetric supercapacitor was assembled by using the $FeCo_2O_4$/Ni foam as electrodes, and PVA/KOH as separator and electrolyte. Fig. 5a shows CV curves of the device between 0 and 1.0 V at various scan rates. The integrated areas increase with the scan rate from 10 mV/s to 100 mV/s. The non-rectangular shape and weak peak indicate a combination of both, pseudocapacitive and electrical double-layer capacitor behaviors. The discharge curves for different current densities are shown in Fig. 5b. The device exhibits high areal capacitances as calculated from the discharge curves: 0.67, 0.59, 0.46, 0.39, and 0.28 F/cm^2 at discharge currents of 2, 3, 5, 8, and 10 mA/cm^2, respectively.

The Ragone plot is shown in Fig. 5c. An energy density of 30.9 Wh/kg is achieved at a power density of 1551 W/kg, and still remains 13.1 Wh/kg at 5240 W/kg (black curve). The specific energy and power densities are superior to those of symmetric supercapacitors with similar electrodes such as

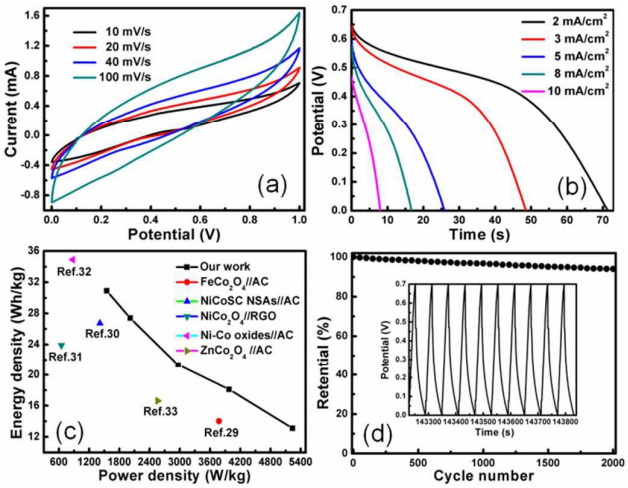

Fig. 5 Electrochemical characterizations of the symmetric capacitor based on our $FeCo_2O_4$/Ni electrodes: (a) CV curves measured at various scan rates, (b) discharge curves at different current densities, (c) Ragone plot with comparison to previous reports of asymmetric devices, and (d) cycling performance over 2000 cycles at 4 mA/ cm^2; the CD curves of the last ten cycles are inset.

$NiCo_2O_4$@polypyrrole (7.5Wh/kg at 500 W/kg)[27] and $NiCo_2O_4$ (8.47 Wh/kg at 1 A/g)[28]. Even the results instead fit together with asymmetric supercapacitor devices based on similar mixed oxides, although asymmetric devices generally perform better than symmetric ones. We compared to asymmetric devices (Fig. 5c) employing activated carbon (AC) and reduced graphene oxide (RGO) as the other electrode, including $FeCo_2O_4$//AC (14 Wh/kg at 3780 W/kg),[29] NiCoSC NSAs//AC (26.74 Wh/kg at 1414.8 W/kg),[30] $NiCo_2O_4$//RGO (23.9 Wh/kg at 650 W/kg),[31] Ni-Co oxides//AC (34.9 Wh/kg at 875 W/kg)[32] and $ZnCo_2O_4$ //AC (16.63 Wh/kg at 2561 W/kg).[33] Galvanostatic CD testing at 4 mA/cm^2 shows that 94% of the initial capacitance remained after 2000 cycles (Fig. 5d), indicating that the $FeCo_2O_4$/Ni foam devices have excellent long-term electrochemical stability. The inset shows the last ten periods, revealing a very regular cycling process.

In conclusion, novel $FeCo_2O_4$ submicron-tube arrays on Ni foams were prepared by a simple template-free chemical growth followed by thermal treatment. The dependence of the microstructures on reactant concentration was investigated and the electrochemical performance thus optimized at $C_{Fe^{3+}}$ = 10 mM. The high porosity, good electric conductivity and strong bonding between the directly grown $FeCo_2O_4$ and the Ni foam lead to outstanding electrochemical performance with a high specific areal capacitance, excellent rate capability (74% retention at 100 mA /cm^2) and excellent cycling stability (91% after 5000 cycles). The assembly of a simple symmetric capacitor led immediately to energy/power densities that surpass other symmetric devices. This obviously demands further research into asymmetric devices with our novel electrodes, which may lead to even better supercapacitors.

Notes and references

1 M. F. El-Kady, V. Strong, S. Dubin and R. B. Kaner, *Science*, 2012, **335**, 1326.
2 Y. K. Hsu, Y. C. Chen, Y. G. Lin, L. C. Chen and K. H. Chen, *Chem. Commun.*, 2011, **47**, 1252.
3 J. Ji, L. Zhang, H. Ji, Y. Li, X. Zhao, X. Bai, X. Fan, F. Zhang and R. Ruoff, *ACS Nano*, 2013, **7**, 6237.
4 H. Jiang, J. Ma and C. Z. Li, *Chem. Commun.*, 2012, **48**, 4465.
5 A. Pendashteh, M. S. Rahmanifar, R. B. Kanerc and M. F. Mousavi, *Chem. Commun.*, 2014, **50**, 1972.
6 G. Zhou, J. Zhu, Y. Chen, L. Mei, X. Duan, G. Zhang, L. Chen, T.Wang and B. Lu, *Electrochim. Acta* 2014, **123**, 450.
7 Z. B. Wu, X. L. Pu , Y. R. Zhu, M. J. Jing, Q. Y. Chen, X. N. Jia and X. B. Ji, *J. of Alloys and Comp.*, 2015, **632**, 208.
8 R. B. Rakhi, W. Chen, M. N. Hedhili, D. Cha and H. N. Alshareef, *ACS Appl. Mater. Interfaces*, 2014, **6**, 4196.
9 K. Wasińskia, M. Walkowiaka, P. Półrolniczaka and G. Lota, *J. Power Sources*, 2015, **293**, 42.
10 S. G. Mohamed, C. J. Chen, C. K. Chen, S. F. Hu and R. S. Liu, *ACS Appl. Mater. Interfaces*, 2014, **6**, 22701.
11 L. Yang, S. Cheng, Y. Ding, X. B. Zhu, Z. L. Wang, M. L. Liu, *Nano Lett.*, 2012, **12**, 321.
12 R. R. Salunkhe, Y. Kamachi, N. L. Torad, S. M. Hwang, Z. Q. Sun, S. X. Dou, J. H. Kim and Y. Yamauchi, *J. Mater. Chem. A*, 2014, **2**, 19848.
13 N. L. Torad, R. R. Salunkhe, Y. Q. Li, H. Hamoudi, M. Imura, Y. Sakka, C. C. Hu and Y. Yamauchi, *Chem. Eur. J.*,2014, **20**, 7895.
14 Le Yu, G. Q. Zhang, C. Z. Yuan and X. W. Lou, *Chem. Commun.*,2013, **49**, 137.
15 R. R. Salunkhe, B. P. Bastakoti, C. T. Hsu, N. Suzuki, J. H. Kim, S. X. Dou, C. C. Hu and Y. Yamauchi, *Chem. Eur. J.* 2014, **20**, 3084.
16 P. H. Yang, Y. Ding, Z. Y. Lin, Z. W. Chen, Y. Z. Li, P. F. Qiang, M. Ebrahimi, W. J. Mai, C. P. Wong and Z. L. Wang, *Nano Lett.*, 2014, **14**, 731.
17 J. P. Liu, J. Jiang, M. Bosmanc and H. J. Fan, *J. Mater. Chem.*, 2012, **22**, 2419.
18 H. C. Chen, J. J. Jiang, L. Zhang, D. D. Xia, Y. D. Zhao, D. Q. Guo, T. Qi and H. Z. Wan, *J. Power Sources*, 2014, **254**, 249.
19 R. Ding, L. Qia, M. J. Jia, H. Y. Wang, *Electrochim. Acta*, 2013, **107**, 494.
20 J. Zhang, J. P. Cheng, M. Li, L. Liu, F. Liu, X. B. Zhang, *J. Electroanal. Chem.*, 2015, **743**, 38
21 J. W. Xiao, L. Wan, S. H. Yang, F. Xiao and S. Wang, *Nano Lett.*, 2014, **14**, 831.
22 M. Li, K.Y. Ma, J. P. Cheng, D. H. Lv, X.B. Zhang, *J. Power Sources*, 2015, **286**, 438.
23 L. B. Kong, C. Lu, M. C. Liu, Y. C. Luo, L. Kang, X. H. Li and F. C. Walsh, *Electrochim. Acta*, 2014, **115**, 22.
24 G. Zhang and W. X. Lou, *Sci. Rep.*, 2013, **3**, 1470.
25 F. Z. Deng, L. Yu, G. Cheng, T. Lin, M. Sun, F. Ye and Y. F. Li, *J. Power Sources*, 2014, **251**, 202.
26 Y. R. Zhu, X. B. Ji, Z. P. Wu, W. X. Song, H. S. Hou, Z. B. Wu, X. He, Q. Y. Chen and C. E. Banks, *J. Power Sources*, 2014, **267**, 888.
27 W. Xiong, X. Hu, X. Wu, Y. Zeng, B. Wang, G. H. He and Z. H. Zhu, *J. Mater. Chem. A,* 2015, **3**,17209.
28 W. Xiong, Y. S. Gao, X. Wu, X. Hu, D. N. Lan, Y. Y. Chen, X. L. Pu, Y. Zeng, J. Su and Z. H. Zhu, *ACS Appl. Mater. Interfaces* 2014, **6**, 19416.
29 A. Pendashteh, J. Palma, M. Anderson and R. Marcilla, *J. Mater. Chem. A*, 2015, **3,** 16849.
30 H. Wang, C. Wang, C. Qing, D. M. Sun, B. X. Wang, G. Qu, M. Sun and Y. W. Tang, *Electrochim. Acta*, 2015, **174**, 1104.
31 V. Chabot, D. Higgins, A.P. Yu, X.C. Xiao, Z.W. Chen and J. J. Zhang, *Energy Environ. Sci.*, 2014, **7**, 1564.
32 J. Zhang, F. Liu, J. P. Cheng and X. B. Zhang, *ACS Appl. Mater. Interfaces*, 2015, **7**, 17630.
33 B. Guan, D. Guo, L. Hu, G. Zhang, T. Fu, W. Ren, J. Li and Q. Li, *J. Mater. Chem. A*, 2014, **2**, 16116.